Charge transfer and asymmetric coupling of $MoSe_2$ valleys to the magnetic order of CrSBr

Caique Serati de Brito,[†,‡] Paulo E. Faria Junior,[¶] Talieh S. Ghiasi,[§] Josep Ingla-Aynés,[§] César Ricardo Rabahi,[†] Camila Cavalini,[†] Florian Dirnberger,[‖] Samuel Mañas-Valero,[§,⊥] Kenji Watanabe,[#] Takashi Taniguchi,[#] Klaus Zollner,[¶] Jaroslav Fabian,[¶] Christian Schüller,[‡] Herre S. J. van der Zant,[§] and Yara Galvão Gobato[*,†]

†*Physics Department, Federal University of São Carlos, São Carlos, SP, 13565-905, Brazil*

‡*Institut für Experimentelle und Angewandte Physik, Universität Regensburg, D-93040 Regensburg, Germany*

¶*Institute for Theoretical Physics, University of Regensburg, 93040 Regensburg, Germany*

§*Kavli Institute of Nanoscience, Delft University of Technology, Lorentzweg 1, 2628 CJ Delft, The Netherlands*

‖*Institute of Applied Physics and Würzburg-Dresden Cluster of Excellence ct.qmat, Technische Universität Dresden, Germany*

⊥*Instituto de Ciencia Molecular (ICMol), Universitat de València, Catedrático José Beltrán 2, Paterna 46980, Spain*

#*Research Center for Materials Nanoarchitectonics, National Institute for Materials Science, 1-1 Namiki, Tsukuba 305-0044, Japan*

E-mail: yara@df.ufscar.br

Sample Preparation and Experimental Methods

The CrSBr crystals were grown by chemical vapor transport and characterized by crystal and powder X-Ray diffraction, Raman and infrared spectroscopy, energy dispersive X-Ray analysis (EDX), high-resolution TEM and SQUID magnetometry[1].The MoSe2 crystal was purchased from SPI Supplies.

The sample consists of a monolayer of $MoSe_2$ on a bulk CrSBr, capped by a thin layer of hexagonal boron nitride (hBN). The monolayer $MoSe_2$, bulk CrSBr and hBN flakes were obtained by mechanical exfoliation on SiO_2 substrates. The thickness of the CrSBr layer is about 35 nm. The heterostructure has been prepared using a dry transfer technique[2]. The hBN layer is picked up by a polycarbonate (PC) film at 70° C, and the hBN is then used to pick up the monolayer $MoSe_2$ and CrSBr flakes successively. The hBN-$MoSe_2$-CrSBr stack is then released on a clean SiO_2 substrate with Au markers by melting the PC layer at temperatures around 180° C. Subsequently, the PC covering the stack is removed from the surface by dissolving it in chloroform and annealed in Ar atmosphere at 150° C for 4 hours. The height profile of the heterostructure is measured by atomic force microscopy, shown in Figure S1.

The micro-PL measurements were performed using a He-flow cryostat (KONTI Micro Cryostat - CryoVac) in the range of temperature 4 K-300 K. We used a spectrometer Acton SP2750 with a coupled PIXIS 100BR eXcelon CCD (Princeton Instruments) and a 532 nm laser. The laser beam was focused onto the monolayer MoSe2 flakes using a 0.7 numerical aperture microscope objective 100X (Nikon).

The magnetic- PL measurements were performed using a helium closed-cycle cryostat with superconducting magnet coils (Attocube - Attodry1000) with magnetic fields up to 9 T applied perpendicular/parallel to the heterostructure. The sample was mounted on Attocube piezoelectric x-y-z translation stages in order to control the sample position. PL measurements were performed using a continuous-wave (cw) laser with a photon energy of 1.88 eV. The PL signal was collimated using an aspheric lens (NA = 0.64) and the selection of

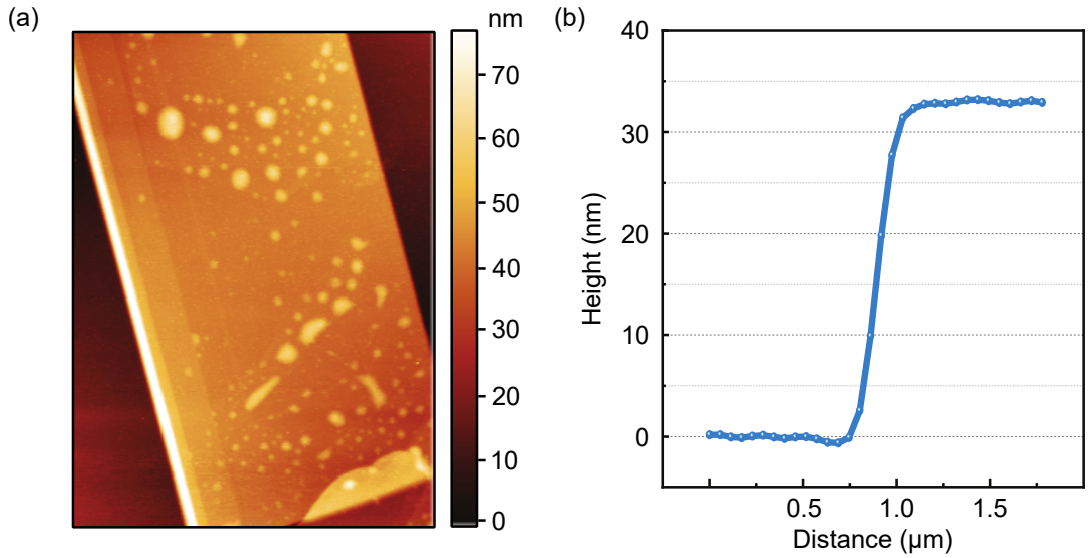

Figure S1: (a) Atomic force microscopy image of the hBN-$MoSe_2$-CrSBr heterostructure on SiO_2, measured in tapping mode. (b) Height profile of the CrSBr flake measured with respect to the SiO_2 substrate.

circular polarization components was performed before to be focused into a 50 μm multimode optical fiber, being dispersed by a 75 cm spectrometer and detected by a silicon CCD detector (Andor, Shamrock/iDus).

Additional Experimental Results

Figure S2 shows the typical PL from different positions of the $MoSe_2$/CrSBr/SiO_2 sample at 4 K. For $MoSe_2$/CrSBr, the exciton and trion emissions are shifted by + 14meV and + 16meV, respectively, as compared to the exciton and trion of $MoSe_2$/SiO_2. Furthermore, the $MoSe_2$/CrSBr PL intensity is much lower (about 4.5 times lower) than the PL intensity from $MoSe_2$/SiO_2 (see Figure S2), indicating some transfer of photocarriers from $MoSe_2$ to CrSBr. In addition, for $MoSe_2$/CrSBr, the trion peak is more intense than the exciton peak, which indicates an increase of doping, as compared to the PL of the $MoSe_2$/SiO_2 region. Furthermore, the linewidth of the exciton on $MoSe_2$/CrSBr is similar to $MoSe_2$/SiO_2, which indicates that the inhomogeneous broadening due to potential fluctuations is similar for both substrates. The linewidth of the trion peak on $MoSe_2$/CrSBr is clearly broader than the

exciton peak in contrast to $MoSe_2/SiO_2$. Small changes in the PL spectrum from different laser positions are also observed, particularly in the heterostructure region, attributed to different local strain distributions and/or doping level. On the other hand, the CrSBr PL peaks are almost unchanged over the whole sample.

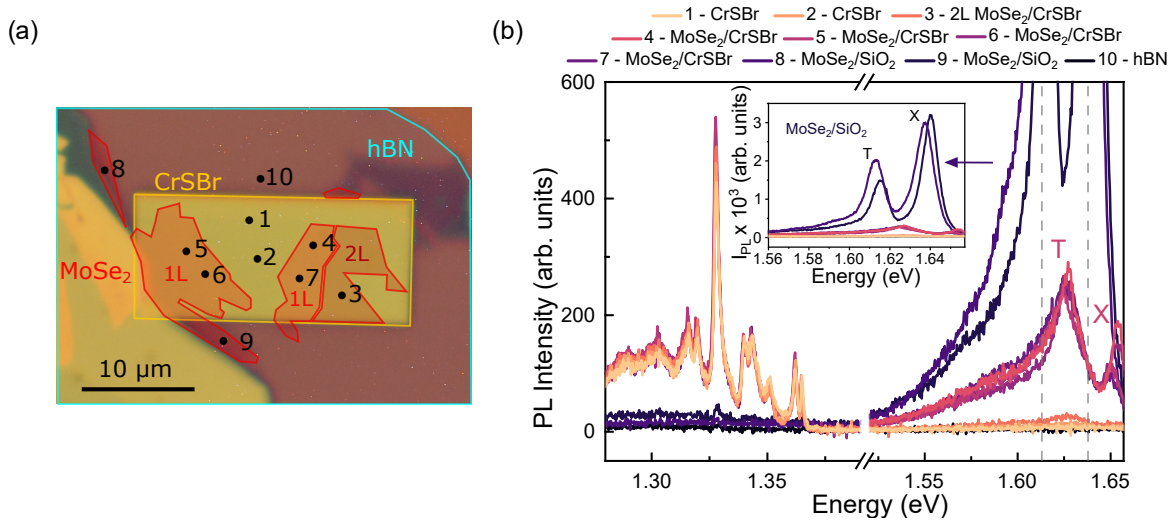

Figure S2: (a) Optical image of the sample (b) typical PL spectra for different positions, labelled by the numbers in (a), at 4 K.

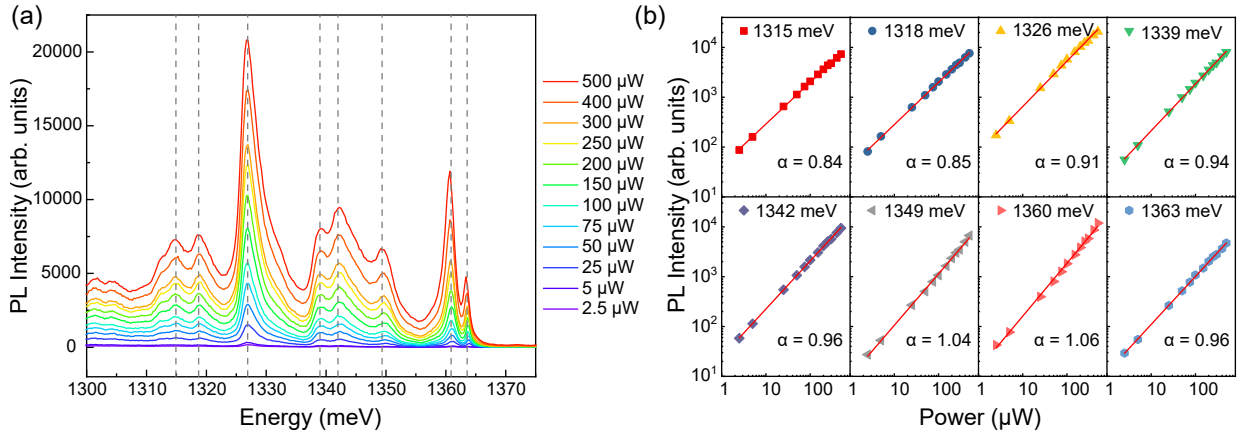

Figure S3: (a) Laser power dependence of the PL spectra from CrSBr. (b) Logarithmic plot of the integrated PL intensity as a function of excitation power for all observed PL peaks. Solid curves show $I \approx P^{\alpha}$ fittings, along with their fitting α values.

Figure S3(a) shows the laser power dependence of the PL spectra of the CrSBr at 4 K. Figure S3(b) shows the double logarithmic plot of the integrated intensities of the different

excitonic peaks as a function of laser power, for several sharp peaks. The solid lines are fitting curves to $I = P^{\alpha}$, along with their respective α values. Ideally, one expects linear behaviour for non-localized excitons, with $\alpha \approx 1$. We have observed that all peaks exhibit a power-law behaviour with α values ≈ 0.8 to 1.0, which would indicate that the nature of these peaks could not be related to localized excitons.

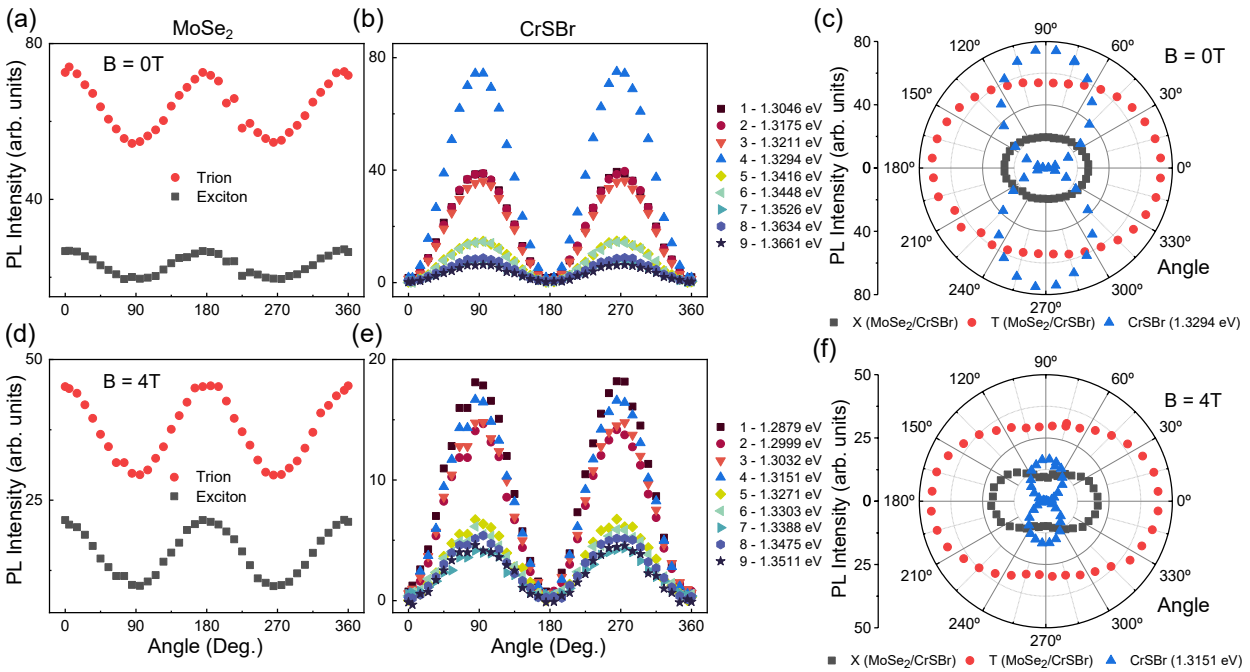

Figure S4: Linear polarization dependence of the peaks of $MoSe_2$ and CrSBr in the antiparallel (AFM) and parallel spin alignment (FM) (out-plane magnetic field at 4 T) of the CrSBr

Figure S4 illustrates the linear polarization resolved PL of $MoSe_2$ and CrSBr under 0T and also under a perpendicular magnetic field of 4 T. This PL dependence with the angle of in-plane polarization evidence the anisotropic photoluminescence from CrSBr and was observed previously regardless of magnetic order (below or above the Néel temperature). Remarkably, the PL of $MoSe_2$ also shows an important dependence with the angle of in-plane polarization which could be explained by magnetic proximity effects. We also observed that this PL angle dependence of $MoSe_2$ is modified under the application of a magnetic field. Figure S5 shows the relative trion/exciton PL intensity for $MoSe_2$/CrSBr and $MoSe_2/SiO_2$ under 0 T and 4 T (after the magnetic field saturation). Interestingly an anomalous angle

dependence is observed for the relative trion/exciton intensity of the PL $MoSe_2$/CrSBr under 4 T which suggests an anisotropic charge transfer between $MoSe_2$ and CrSBr.

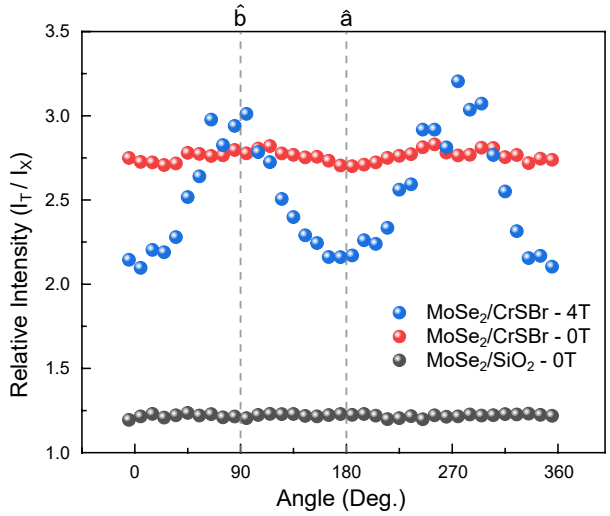

Figure S5: Relative trion/exciton PL intensity (I_T/I_X) of the $MoSe_2$ as a function of the in-plane polarization angle for 0 T and out-plane magnetic field of 4 T.

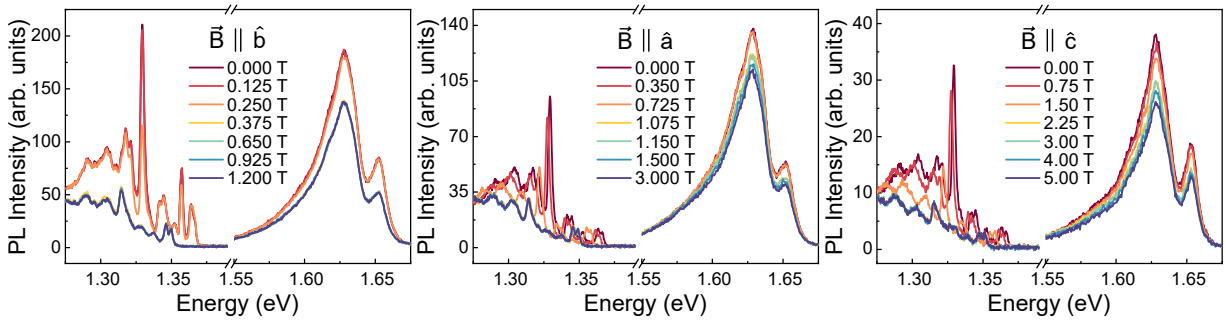

Figure S6: PL Spectra of the $MoSe_2$/CrSBr sample for selected magnetic field values applied parallel to the easy, intermediary and hard axis of CrSBr, respectively.

Figure S6 show typical PL spectra for selected magnetic fields for different crystal orientations. It shows an abrupt change for the PL peak positions of CrSBr and PL intensity of $MoSe_2$ for the magnetic field parallel to the easy axis. In contrast, a smooth change is observed for the PL peak positions of CrSBr and PL intensity of $MoSe_2$ under a magnetic field parallel to the intermediate and hard axis.All sharp PL peaks from the CrSBr show similar behaviour and allows to probe the magnetic phase transitions in CrSBr.

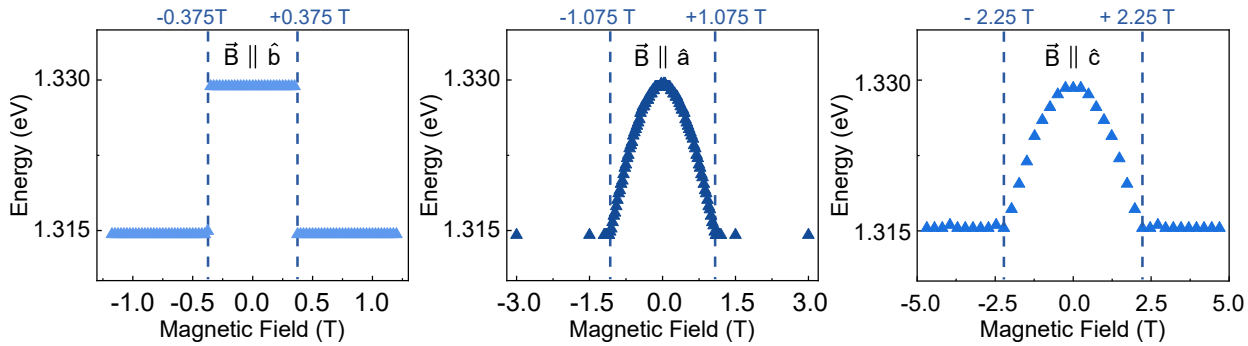

Figure S7: Magnetic field dependence of the most intense CrSBr peak energy, for $\vec{B}$ applied in all the 3 axes. The saturation field in each case is shown by the dashed lines.

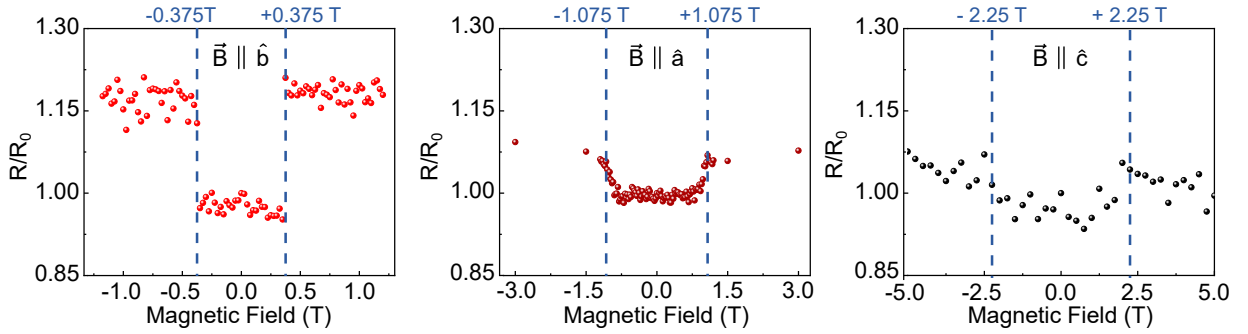

Figure S8: Relative trion/exciton PL intensity ($R = I_T/I_X$) of the $MoSe_2$, under a magnetic field applied parallel to the (a) easy axis, (b) intermediary and (c) hard axis. R was normalized by the B = 0 T value (R_0)

Figure S8 shows the relative trion/exciton PL intensity of as a function of magnetic field. We observed a clear correlation between the trion/exciton relative PL intensity versus magnetic field in $MoSe_2$ with the PL peak position dependence of CrSBr versus magnetic field. Particularly, an abrupt change of R is observed around 0.375 T (same saturation field for the PL peak energy of CrSBr) for B parallel to the easy axis. On the other hand, an smooth variation with the same saturation field for CrSBr is also observed for B parallel to the other crystal orientations. These results indicate that the observed changes of the $MoSe_2$ PL intensity could be related to changes in the band offset between the CrSBr and $MoSe_2$ layers after the B induced change of phase order of CrSBr. This effect could modify the charge transfer between the layers and explain our PL results.

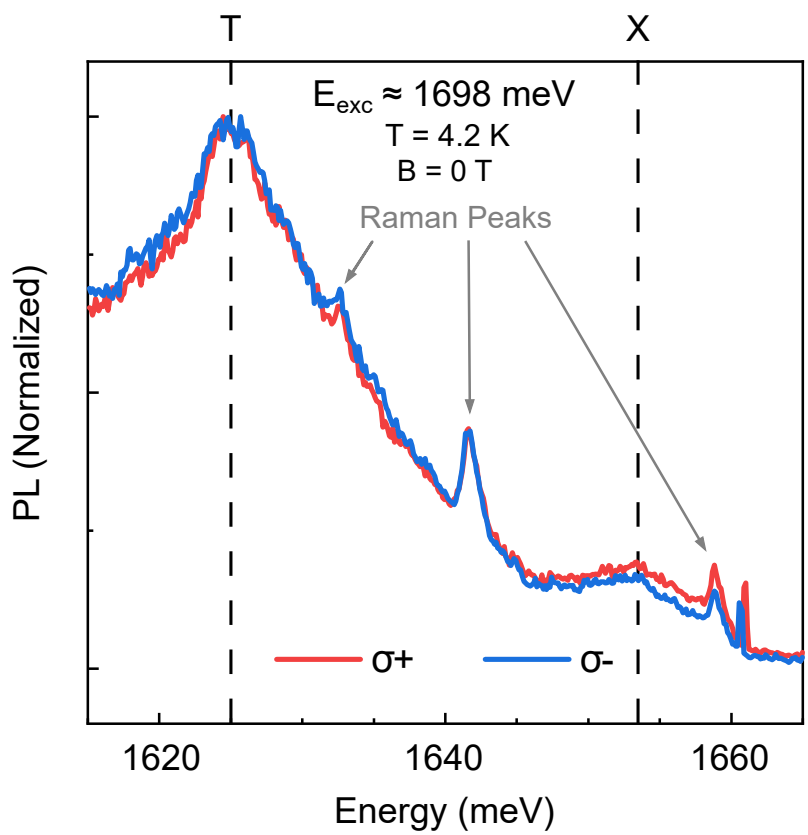

Figure S9: σ^+ and σ^- PL spectra at low temperature and under zero magnetic field for the $MoSe_2$/CrSBr heterostructure. The excitation energy is 1698 meV (730 nm).

Figure S9 shows the σ^+ and σ^- PL spectra at 3.6 K, and zero magnetic field using a

730 nm linear polarized laser.The exciton (X) and trion (T) peaks are indicated in the figure. Due to the resonant excitation, some Raman peaks can also be observed in the PL spectra. We have not observed any energy valley splitting under zero magnetic field as expected.

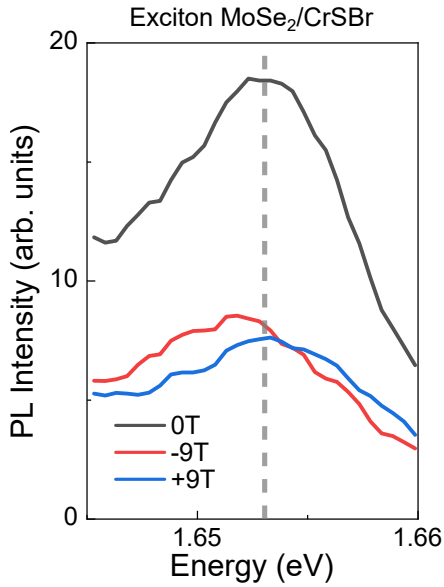

Figure S10: PL spectra of $MoSe_2$/CrSBr in the spectral region of the exciton peak at 0 T, -9 T and +9 T.

Fig. S10 shows the circular polarized resolved PL spectra at 0 T, -9 T and +9 T. We clearly observed a Zeeman shift asymmetry. Fig. S11 shows the circularly resolved PL spectra and fittings for selected values of magnetic fields. The magnetic field dependence of the Full Width at Half Maximum (FWHM) for exciton and trion peaks in $MoSe_2$/CrSBr are also shown.

The fittings were carried systematically, analyzing the PL spectra for the magnetic field interval of 0.25 T. The fittings were performed using four Voigt functions. The extracted g-factors and error bars were obtained from the magnetic field dependence of the Zeeman shift (Fig. 3) and are shown in Table I of the manuscript. The error bars depend on the range of applied magnetic fields. Particularly for lower magnetic field (AFM ordering, i.e., $\left|\vec{B}_{\hat{c}}\right| < 2.25$ T) these error bars are higher.

In addition, we remark that the FWHM has small impact on the error bar values. Partic-

ularly, no relevant FWHM variation was observed in the magnetic field dependence for the exciton peak. This result suggests that the primary sources of error in our measurements are associated with other factors, such as the dispersion of the data related to linear regression, which validate our estimations.

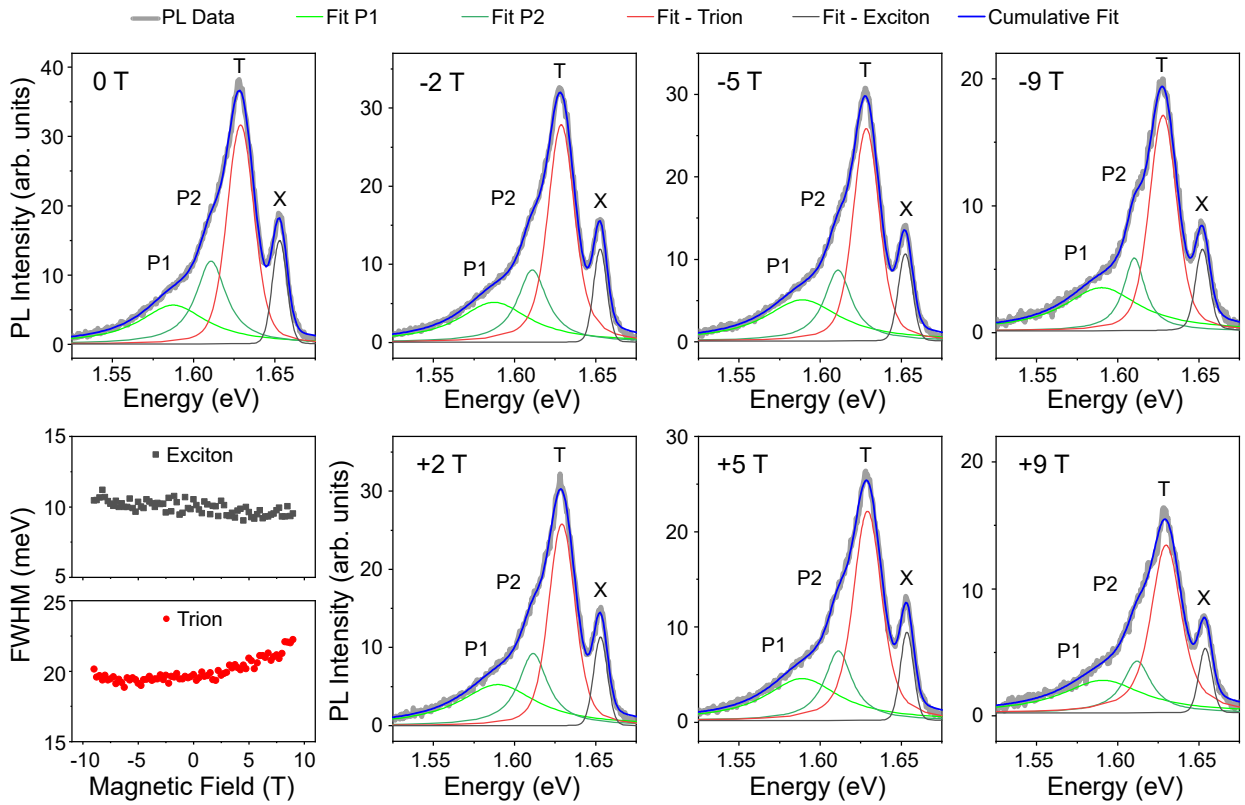

Figure S11: Typical PL spectra and fittings for selected magnetic fields (-9 T, -5 T, -2 T, 0 T, +2 T, +5 T and +9 T). For optimal fitting to data, four Voigt functions were employed (P1, P2, X and T). The bottom-left panels shows the magnetic field dependence of the FWHM for the exciton and trion peaks.

Figure S12 shows the magnetic field dependence of the Zeeman shift for the trion peak in $MoSe_2/SiO_2$ and $MoSe_2/CrSBr$.

Figure S13 shows the normalized PL spectra for different temperatures for CrSBr and also for the $MoSe_2$ on both CrSBr and SiO_2 substrates.

For $MoSe_2/SiO_2$ we observed a standard temperature dependence for both exciton and trions in agreement with previous measurements in the literature. We extracted a trion bind-

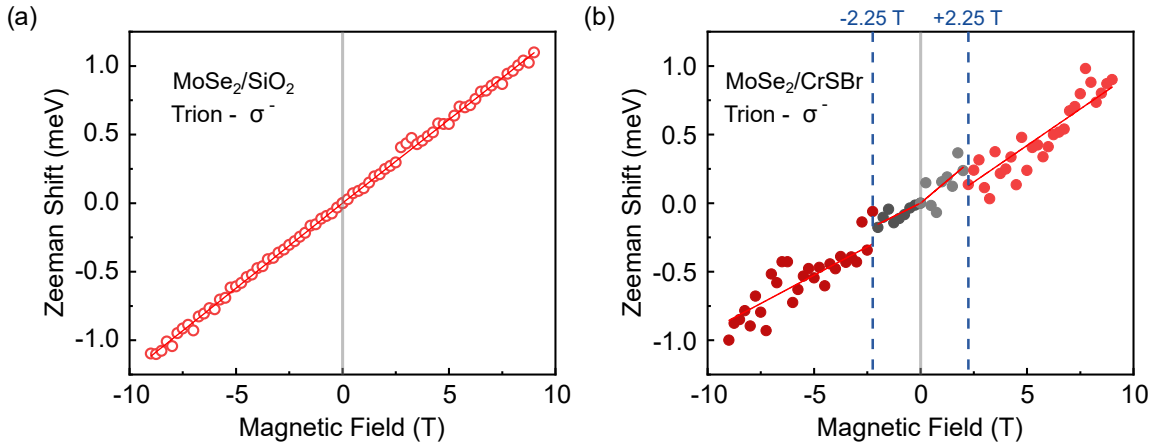

Figure S12: Trion Zeeman shift obtained from the fittings of the σ^- PL spectra with an out-of-plane magnetic field, ranging from -9 T to 9 T. The solids lines are the linear functions that best fit the data. The g-factor values are shown in Table I of the manuscript.

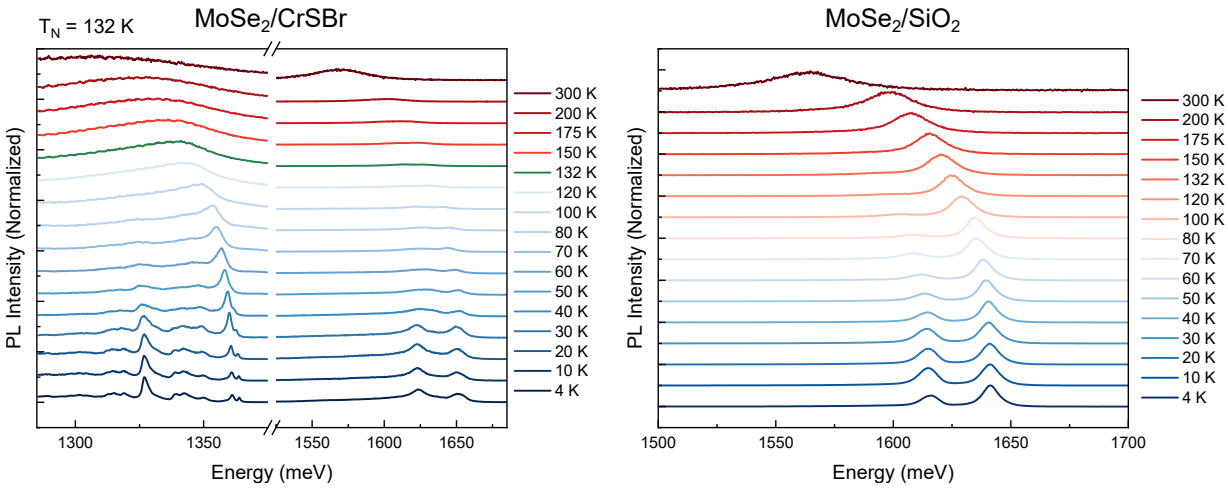

Figure S13: Normalized PL spectra for different temperatures for CrSBr and $MoSe_2$ for the $MoSe_2$/CrSBr and $MoSe_2/SiO_2$

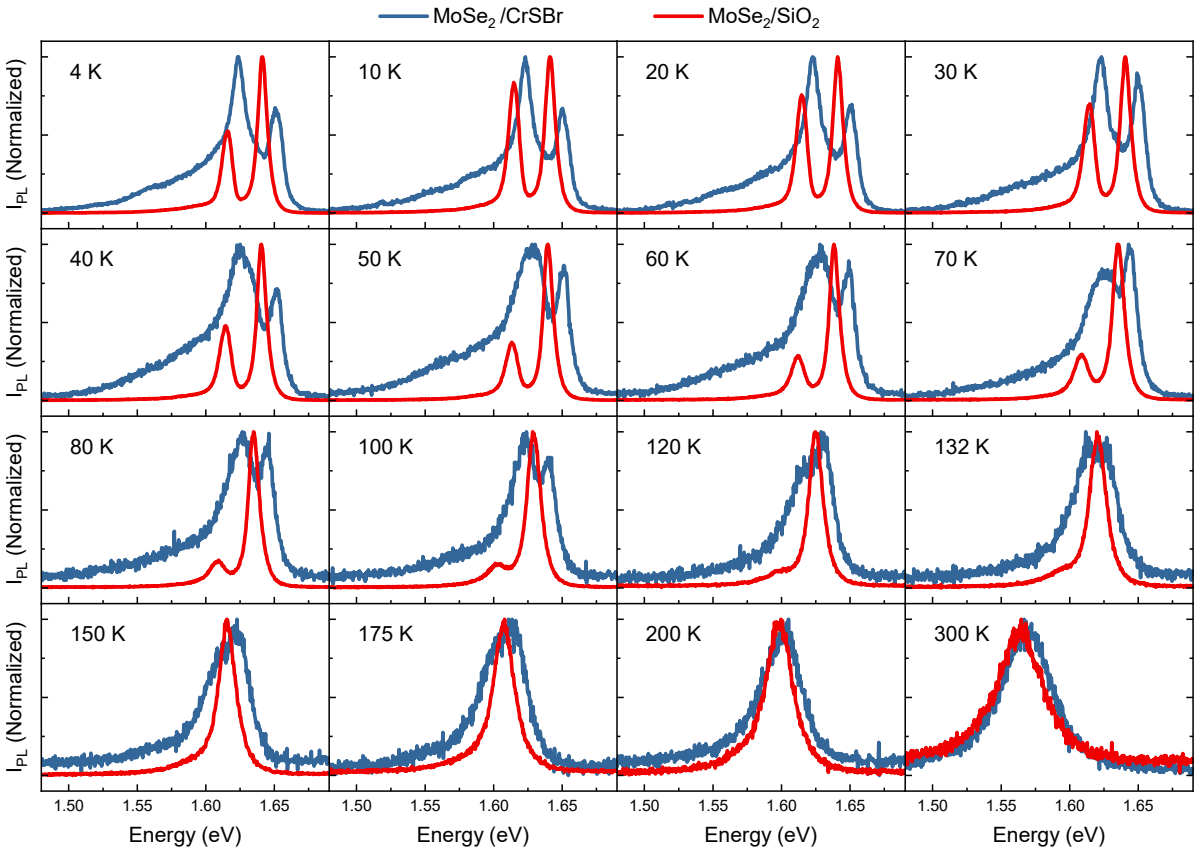

Figure S14: Normalized $MoSe_2$ PL spectra for different temperatures for $MoSe_2$/CrSBr and $MoSe_2/SiO_2$

ing energy of around 27 meV which does not change with the increase of the temperature as expected. Actually, the PL peak positions of the exciton and trion emissions follow the standard bandgap shrinkage of $MoSe_2$ with increasing temperature. On the other hand a different behaviour is observed for the temperature dependence of the PL from $MoSe_2$/CrSBr. Figure S14 shows the normalized PL of $MoSe_2$ on CrSBr and on SiO_2 for different temperatures in the range of 4 K to 300 K. We observed an anomalous dependence for the $MoSe_2$ PL peak positions and trion binding energy for $MoSe_2$/CrSBr between the magnetic phase transitions of CrSBr (40 K to 132 K). We clearly remark that for the $MoSe_2$/CrSBr region, the trion binding energy changes with the temperature between the temperature of these magnetic phase transitions.

Density functional theory and band alignment

In order to have an insight into the possible band alignment between $MoSe_2$ and bulk CrSBr, we investigate the band edges with respect to the vacuum level and the band gaps within first principles as a function of the number of layers of CrSBr without spin-orbit coupling (SOC) and considering the FM phase. Our calculations shown in Figure S15 indicate that 6L is a good approximation for bulk CrSBr since the energy levels are nearly converged. Furthermore, our results are nearly independent on the choice of the U parameter. This particular band offset indicates that $MoSe_2$ would be slightly p-doped, forming a type-III band alignment with bulk CrSBr. In the main text of the manuscript, SOC is included in the calculations and the type-III band alignement is maintained.

The first principles calculations were performed within the density functional theory implemented in WIEN2k[3]. We used the Perdew–Burke–Ernzerhof[4] exchange-correlation functional. we employed Hubbard U = 2 and 3 eV[5], as well as DFT-D3 van der Waals corrections[6]. The wavefunction expansion into atomic spheres takes into account orbital quantum numbers up to 10 and the plane-wave cut-off multiplied with the smallest atomic

radii is set to 9. Spin–orbit coupling was included fully relativistically for core electrons, while valence electrons were treated within a second-variational procedure[7] with the scalar-relativistic wavefunctions calculated in an energy window up to 1.9 Ry. Self-consistency was achieved using a two-dimensional Monkhorst–Pack k-grid with 15×15 points for $MoSe_2$, and 28×20 points for CrSBr systems, and the convergence criteria of 10^{-6} e for the charge and 10^{-6} Ry for the energy. For $MoSe_2$, we used a lattice parameter of 3.289 Å and thickness of 3.335 Å[8]. For CrSBr, we employed experimentally determined lattice constants[9,10]. A vacuum region of 16 Å was considered to avoid interaction between the heterostructure replicas.

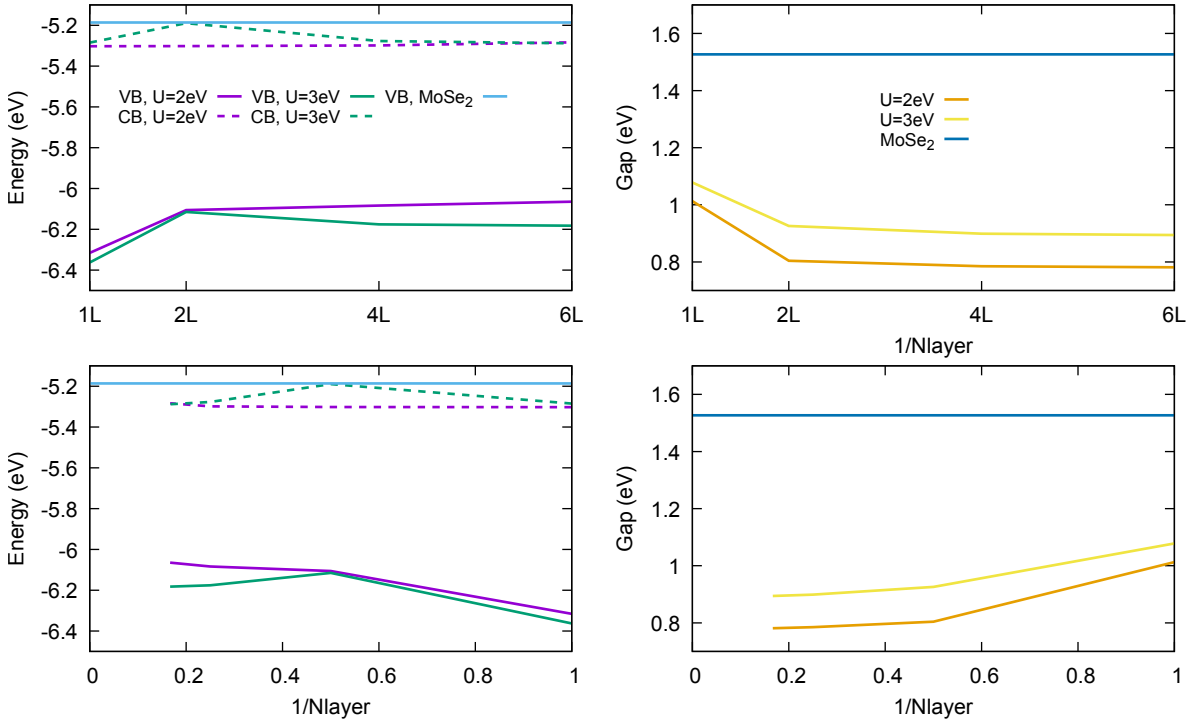

Figure S15: Density functional theory calculations of the relevant energy levels in multilayer CrSBr. Left column: conduction band (CB) and valence band (VB) with respect to the vacuum level. Right column: band gaps.

References

(1) Boix-Constant, C. et al. Probing the Spin Dimensionality in Single-Layer CrSBr Van Der Waals Heterostructures by Magneto-Transport Measurements. *Advanced Materials* **2022**, *34*, 2204940.

(2) Zomer, P. J.; Guimarães, M. H. D.; Brant, J. C.; Tombros, N.; van Wees, B. J. Fast pick up technique for high quality heterostructures of bilayer graphene and hexagonal boron nitride. *Applied Physics Letters* **2014**, *105*, 013101.

(3) Blaha, P.; Schwarz, K.; Tran, F.; Laskowski, R.; Madsen, G. K.; Marks, L. D. WIEN2k: An APW+lo program for calculating the properties of solids. *The Journal of Chemical Physics* **2020**, *152*, 074101.

(4) Perdew, J. P.; Burke, K.; Ernzerhof, M. Generalized Gradient Approximation Made Simple. *Physical Review Letters* **1996**, *77*, 3865.

(5) Wang, H.; Qi, J.; Qian, X. Electrically tunable high Curie temperature two-dimensional ferromagnetism in van der Waals layered crystals. *Applied Physics Letters* **2020**, *117*.

(6) Grimme, S.; Antony, J.; Ehrlich, S.; Krieg, H. A consistent and accurate ab initio parametrization of density functional dispersion correction (DFT-D) for the 94 elements H-Pu. *The Journal of Chemical Physics* **2010**, *132*, 154104.

(7) Singh, D. J.; Nordstrom, L. *Planewaves, Pseudopotentials, and the LAPW method*; Springer Science & Business Media, 2006.

(8) Kormányos, A.; Burkard, G.; Gmitra, M.; Fabian, J.; Zólyomi, V.; Drummond, N. D.; Fal'ko, V. k · p theory for two-dimensional transition metal dichalcogenide semiconductors. *2D Materials* **2015**, *2*, 022001.

(9) Telford, E. J.; Dismukes, A. H.; Lee, K.; Cheng, M.; Wieteska, A.; Bartholomew, A. K.; Chen, Y.-S.; Xu, X.; Pasupathy, A. N.; Zhu, X.; Dean, C. R.; Roy, X. Layered Anti-

ferromagnetism Induces Large Negative Magnetoresistance in the van der Waals Semiconductor CrSBr. *Advanced Materials* **2020**, *32*, 2003240.

(10) Telford, Evan J.; Dismukes, Avalon H.; Lee, Kihong; Cheng, Minghao; Wieteska, Andrew; Bartholomew, Amymarie K.; Chen, Yu-Sheng; Xu, Xiaodong; Pasupathy, Abhay N.; Zhu, Xiaoyang; Dean, Cory R.; Roy, Xavier CSD 2006679: Experimental Crystal Structure Determination. 2021; `http://www.ccdc.cam.ac.uk/services/structure_request?id=doi:10.25505/fiz.icsd.cc25c3l8&sid=DataCite`.